Effects of Restricted Rotations and Dynamic Averaging on the Calculated Isotropic Hyperfine Coupling Constants of the *bis*-Dimethyl and *bis*-Di(trifluoromethyl) Nitroxide Radicals

Saba M. Mattar* and Jacob Sanford

University of New Brunswick, Department of Chemistry and Centre for Laser, Atomic and Molecular Sciences, Fredericton, New Brunswick, Canada E3B 6E2

Received: August 8, 2009

The rotational effects of the CH_3 and CF_3 groups on the electronic structure and nuclear hyperfine coupling constants (HFCCs) in dimethylnitroxide (**DMNO·**) and ditrifluoro-methynitroxide (**TFMNO·**) are investigated using the UB1LYP hybrid density functional method. The CH_3 and CF_3 HFCCs of both radicals are found to obey the McConnell relation during rotation. The two CH_3 groups of the **DMNO·** do not gear with each other, but the rotation of the first CH_3 group induces only a small rocking effect (~7°) in the second group. However, in **TFMNO·**, the fluorine atoms from different CF_3 groups are close enough so that the steric repulsion between them causes them to act as two interlocked gears, where one drives the other. Therefore, both CF_3 groups undergo full rotation. To the best of our knowledge, this is only the second example of "gearing" to be studied. Stabilization due to hyperconjugation is also a major factor that affects the magnitudes of the HFCCs of the CF_3 groups during rotational averaging. Stable configurations at specific CF_3 group orientations have a large overlap with the NO π-electron cloud because the lobes of the hybridized $p_\sigma(F_2)$, $p_\sigma(F_3)$, $p_\sigma(F_5)$, and $p_\sigma(F_6)$ orbitals along the F−C bonds have cylindrical symmetry and are of the correct phases for hyperconjugation to occur. The calculated **TFMNO·** C_1−N and C_2−N bond orders range from 0.91 to 0.95 as the CF_3 groups are rotated. Therefore, the C−N bonds are essentially single bonds. This, in conjunction with the low rotational energy barrier of approximately 50 cm^{-1}, explains why the EPR intensities of the ^{19}F hyperfine splittings, in the range of 163−297 K, are characteristic of six equivalent rapidly rotating fluorine atoms. The **TFMNO·** out-of-plane NO vibrations induce additional s character at the ^{14}N nucleus. This increases the magnitude of the ^{14}N HFCC and decreases the ^{19}F HFCCs. As the temperature increases and because of mixing of the first excited out-of-plane vibrational state, the NO vibrational amplitudes also increase. This leads to an increased ^{14}N HFCC and decreased ^{19}F HFCCs, which is in agreement with experiment.

1. Introduction

Nitroxide spin labels are persistent free radicals. The first nitroxide radical prepared was the nitrosyl disulfonate anion of Fremy's salt.[1] Since then, hundreds of nitroxide radicals have been synthesized and are widely used in the fields of chemistry, biochemistry, biophysics, electron paramagnetic resonance (EPR), and electron nuclear double resonance (ENDOR) spectroscopy.[2−6]

The *bis*-(trifluoromethyl) nitroxide (**TFMNO·**), shown in Figure 1, is a stable neutral free radical. When pure, it is a yellow solid at cryogenic temperatures. From 203 to 248 K, it is a liquid, and above that range, it is a purple gas. The radical has been characterized by infrared, nuclear magnetic resonance, and EPR spectroscopies.[7] The EPR signal intensity of a 30% solution of **TFMNO·** in chloroform gradually decreases as the temperature is lowered from 298 to 113 K. This indicates that in solution, **TFMNO·** dimerizes at low temperatures. From this data, its heat of dimerization, ΔH, was estimated to be −2.5 kcal/mol.[7] The radical's nitrogen isotropic hyperfine coupling constant, $a^{iso}(^{14}N)$, obtained from EPR at room temperature was found to be 9.3 Gauss (G), whereas that of the six rotationally averaged fluorines, $\langle a^{iso}(^{19}F)\rangle$, was 8.2 G.[7]

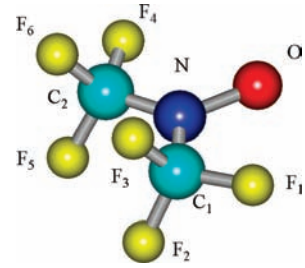

Figure 1. Chemical structure and atomic numbering of **TFMNO·**. The fluorine atoms of the first CF_3 group are labeled F_1, F_2, and F_3, whereas those of the second CF_3 group are F_4, F_5, and F_6.

The stability of **TFMNO·** was attributed to the strong electronegativity of its two CF_3 groups, which attract the unpaired electron density away from the NO moiety and delocalize it over the whole molecule.[7] The nonzero value $\langle a^{iso}(^{19}F)\rangle = 8.2$ G is unequivocal experimental proof that there is a net spin density at each of the six fluorine nuclei. In addition, the small value of $a^{iso}(^{14}N) = 9.3$ G compared with other nitroxide radicals (~14 G) corroborates the fact that the N atom has less than normal net spin density. The issue at the time was to understand the mechanism of this delocalization and how it affects the rotation of the two CF_3 groups.[7]

* Corresponding author. E-mail: mattar@unb.ca. Tel: +1(506) 447 3091. Fax: +1(506) 453 4981.

10.1021/jp9076646 CCC: $40.75
Published on Web 09/21/2009

Scheidler and Bolton, in an attempt to determine the delocalization mechanism, measured $a^{iso}(^{14}N)$ and $\langle a^{iso}(^{19}F)\rangle$ over a temperature range extending from 163 to 297 K.[8] As the temperature was raised, the magnitude of $a^{iso}(^{14}N)$ increased, whereas that of $\langle a^{iso}(^{19}F)\rangle$ decreased. Their fit of the data showed that $a^{iso}(^{14}N)$ and $\langle a^{iso}(^{19}F)\rangle$ obey the empirical relations

$$a^{iso}(^{14}N) = 8.776 + 0.0023T \quad (1)$$

$$\langle a^{iso}(^{19}F)\rangle = 9.327 - 0.0036T \quad (2)$$

They considered these results to be "anomalous" and to explain this behavior, they proposed a direct 1−3 conjugation between the NO π-electron cloud and the CF_3 fluorine p orbitals.[8] The proposed 1−3 electron conjugation mechanism implies that, in principle, the CN bonds have some partial double bond character. This, in turn, will lead to hindered rotation about these bonds. The EPR intensities of the fluorine hyperfine splittings obey a binomial distribution characteristic of six equivalent fluorine atoms. To rationalize these apparent discrepancies, Scheidler and Bolton proposed that although partial hindered rotation may occur, the CF_3 rotational energy barrier must be small, and the rotation rate must be much larger than 2.5×10^7 sec^{-1}.[8]

The accurate calculation of the isotropic hyperfine coupling constants is one of the most difficult tasks in computational chemistry,[9] and hence the verification of the Scheidler and Bolton postulates remained an open question. Nevertheless, with the advent of hybrid density functional techniques, it has become possible not only to calculate hyperfine coupling constants accurately but also to take into consideration the effects of vibrational and rotational averaging.[10] For most nitroxide spin labels, excellent agreement between computed and experimental hyperfine and **g** tensors is obtained.[9−12]

The temperature dependence of the experimental $a^{iso}(^{14}N)$ and $\langle a^{iso}(^{19}F)\rangle$ strongly suggests that molecular motion and dynamical effects, such as vibrational and rotational averaging, play an important role in interpreting the**TFMNO·** EPR spectra. Our interest in rotational averaging commenced with the 4,5-bis-(trifluoromethy) −1,3,2-dithiazol-2-yl (**BG·**) radical.[13] Detailed theoretical, computational, and experimental investigations led to the thorough understanding of its electronic structure, nuclear hyperfine couplings constants, and **g** tensors. In the **BG·** case, extensive calculations indicated that the rotation of one CF_3 group affects the rotation of the second CF_3, resulting in correlated rotational (CR) averaging.[13] The two CF_3 groups of **BG·** are separated by two carbon atoms, whereas, in the case of **TFMNO·**, the two CF_3 groups are even closer to one another because they both form C−N bonds with the same nitrogen atom, as shown in Figure 1. Therefore, the influence of rotation of one CF_3 group on the second may even be much more prominent in the **TFMNO·** case. One of the main aims of this article is to study the effects of CR averaging of the two CF_3 groups on the electronic and magnetic properties of **TFMNO·**.

The effect of the vibrational bending modes due to the oxygen atom displacement out of the CNC plane in nitroxide radicals is also known to affect the magnitudes of their $a^{iso}(^{14}N)$.[9,10,14] The unpaired electron of a nitroxide radical formally resides on the oxygen atom.[14] However, because of its stronger electronegativity, the oxygen atom will attract some additional electron density from its neighboring nitrogen atom. This induces a net spin density on the nitrogen that, in turn, is responsible for a nonzero $a^{iso}(^{14}N)$. If the two carbon, nitrogen and oxygen atoms all lie in the same plane, then $a^{iso}(^{14}N)$ is entirely due to core polarization from its out-of-plane $2p_z(N)$ atomic orbital. However, if the oxygen atom bends out of the CCN plane, then the nitrogen atom will also acquire some s(N) character, which will additionally contribute to its net spin density at its nucleus and increase $a^{iso}(^{14}N)$. In the **TFMNO·** case, this could be an important factor in the behavior of $a^{iso}(^{14}N)$ as the temperature is varied. Therefore, in this article, the out-of-plane NO vibrations and their effect on $a^{iso}(^{14}N)$ and $\langle a^{iso}(^{19}F)\rangle$ are also investigated.

TABLE 1: Criteria and Tolerances for Geometry Optimization

parameter change (au)	tolerance
energy	5.0×10^{-6}
root mean square gradient	1.0×10^{-4}
maximum gradient	3.0×10^{-3}
root mean square displacement	2.0×10^{-3}
maximum displacement	4.0×10^{-3}

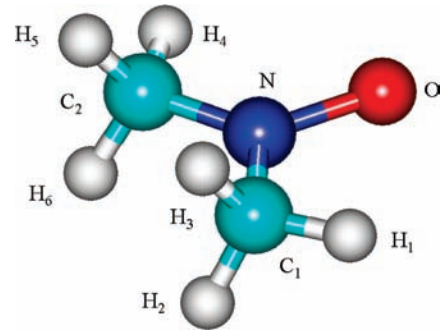

Figure 2. Atomic numbering of the **DMNO·** neutral radical. The hydrogen atoms of the two methyl groups are labeled in the same fashion as the **TFMNO·** CF_3 groups.

2. Computational Details

The ORCA suite of programs[15] was used for the electronic structure and nuclear hyperfine tensor computations. The geometry of the **TFMNO·** and $(CH_3)_2NO$ (**DMNO·**) radicals was first optimized using the UB1LYP[16−18] method and EPR-II basis sets of Barone.[12,19] The atomic coordinates of the geometry-optimized radical were subsequently used as input to perform relaxed scans. After each relaxed scan, the total energy and the nuclear hyperfine tensor (**A**) were calculated. The EPR-II basis sets were specifically chosen for the computation of the hyperfine tensors because of their very tight s functions.[19] The relaxed scan geometry optimizations were terminated when the changes in a set of five parameters were all less than their assigned tolerances.[15] The parameters and their tolerances are given in Table 1.

3. Results and Discussion

3.1. Interaction of Methyl Groups in Dimethyl Nitroxide. To understand the influence of one CF_3 group on the other one in **TFMNO·**, it was deemed necessary to first study the simpler **DMNO·** radical, shown in Figure 2. Just as in the case of **TFMNO·**, the two **DMNO·** CH_3 groups are connected to the same nitrogen atom and quite close. Therefore, the rotation of one CH_3 group may affect the other.

The **DMNO·** relaxed scans entailed setting the H_1C_1NO dihedral angle, $\varphi_{H_1C_1NO}$, to 0°, and the C_1, C_2, N, and O atoms were all constrained to lie in the same plane, as shown in Figure 2. All remaining internal coordinates were then optimized. H_4

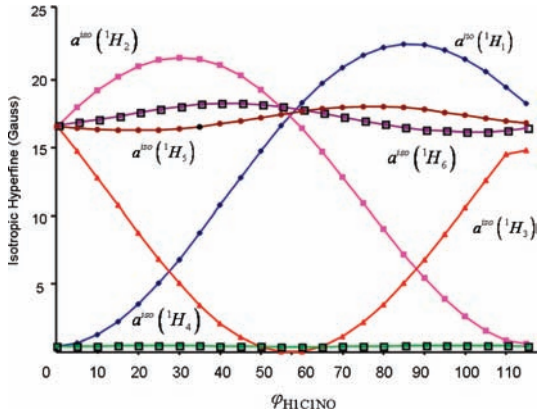

Figure 3. Effect of rotation of one CH_3 group on the six $a^{iso}(^1H)$ of the **DMNO·** radical.

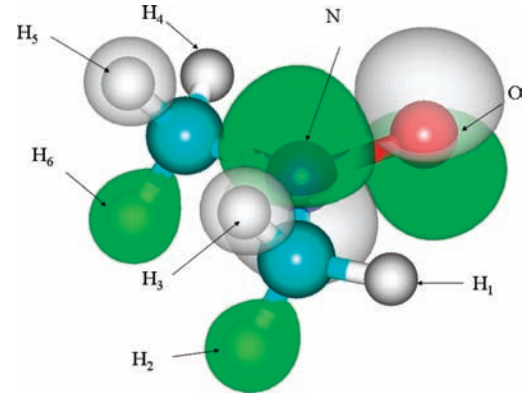

Figure 4. Three-dimensional isosurface of the **DMNO·** highest singly occupied molecular orbital (SOMO). Green surfaces have a positive phase, whereas white surfaces are negative. Both molecules in Figures 2 and 4 have the same orientation.

was also found to lie in this plane. In addition, H_3 and H_5 lie above the plane, whereas H_2 and H_6 lie below it. After this partial optimization, the $a^{iso}(^{14}N)$ and six $a^{iso}(^1H)$ were calculated using the UB1LYP hybrid density functional and Barone's EPR-II basis sets. The $\varphi_{H_1C_1NO}$ dihedral angle was then incremented by 5°, and the entire process was repeated again. In this manner, $\varphi_{H_1C_1NO}$ was scanned from 0 to 120°.

Figure 3 depicts the effect of the rotation of one methyl group on the six isotropic hyperfine coupling constants of the hydrogen atoms. As the first CH_3 group is rotated by 120°, $a^{iso}(^1H_1)$, $a^{iso}(^1H_2)$, and $a^{iso}(^1H_3)$ vary in a periodic manner. The variation of the three hydrogen hyperfine coupling constants is found to obey the McConnell relation, given as[20]

$$a^{iso}(^1H_j) = \{B_0 + B_1 \cos^2[\theta + 60(j-1)]\}\rho(j) \quad (3)$$

where $j = 1, 2, 3$ and $\rho(j)$ is the electron charge density at the jth nucleus.

The proportionality constant, B_0, is due to core polarization and is independent of orientation effects. In contrast, the B_1 factor arises mainly from hyperconjugation. In eq 3, θ is the angle made between the NCH_j plane and the $2p_z(N)$ orbital that is perpendicular to the C_1NC_2 plane in Figure 2. Inspection of the data in Figure 3 indicates that the constants B_0 and B_1 in eq 3 for this radical are approximately −1.1 and 44.0 G, respectively. This $\cos^2(\theta)$ dependence is similar to what was found previously when the ortho methyl group of the *para*-semiquinone underwent free rotation.[21]

In the strictest sense, eq 3 applies only if the radical has one methyl group. In that case, $a^{iso}(^1H_1)$ and $a^{iso}(^1H_2)$ should display maxima at 90 and 30°, respectively. $a^{iso}(^1H_3)$ should display a minimum at 60°. In addition, $a^{iso}(^1H_1)$ and $a^{iso}(^1H_2)$ should also intersect at 60°. However, close inspection of Figure 3 shows that $a^{iso}(^1H_1)$, $a^{iso}(^1H_2)$, and $a^{iso}(^1H_3)$ are slightly off by ∼2°. This could be due to the small perturbation from the second CH_3 group or computational inaccuracies due to finite geometry optimization tolerances. One may assume that the presence of the second CH_3 group has a very minor effect on the hyperfine coupling constants of the first CH_3 group. Consequently, the variation of the isotropic hyperfine coupling constants of H_1, H_2, and H_3 with $\varphi_{H_1C_1NO}$ is generally well understood and displays no anomalies.

The **DMNO·** partially optimized geometries show that varying the $\varphi_{H_1C_1NO}$ of the first CH_3 group induces only a slight rocking effect of ∼7° in the second CH_3 group. Therefore, the two methyl groups do not "gear" with one another. The slight variations in the H_4C_2NO, H_5C_2NO, and H_6C_2NO dihedral angles, because of rocking, cause minor variations in $a^{iso}(^1H_5)$ and $a^{iso}(^1H_6)$, as illustrated in Figure 3. The results are also consistent with a B_1 of 44.0 G when substituted into eq 3 with $j = 5, 6$.

It is worth noting that in Figure 3, the observed change of $a^{iso}(^1H_4)$ is very small because H_4 lies in the C_1NO plane, and consequently, the angle $\theta \approx 90°$. This causes the $\cos^2\theta$ term in eq 3 to be approximately zero, and the only contribution to $a^{iso}(^1H_4)$ is due to B_0. Because the first methyl group is rotated from 0 to 120°, the induced rocking in the second methyl group causes the angle θ for H_4 to change from 86 to 94°. This causes the $B_1 \cos^2[\theta + 60(j-1)]$ term in eq 3 to vary by 0.17 G, which is very close to what is observed in Figure 3. In the case of $a^{iso}(^1H_5)$ and $a^{iso}(^1H_6)$, the change in θ, due to rocking, is from 206 to 214° and 326 to 334°, respectively. Therefore, the $B_1 \cos^2[\theta + 60(j-1)]$ term is not small, and they experience a much larger variation in their magnitudes compared with $a^{iso}(^1H_4)$.

In summary, in the **DMNO·** case, the effect of rotation of one CH_3 group on the other, while not negligible, is of minor importance.

Finally, an inspection of the **DMNO·** singly occupied molecular orbital (SOMO) in Figure 4 reveals the significant role of hyperconjugation. The delocalization of the SOMO, formally from the NO moiety, to the two methyl groups is quite evident. In the particular configuration shown in Figure 4, H_1 and H_4 lie in the plane containing the C_1, C_2, N, and O atoms and have no out-of-plane π character. In contrast, the s atomic orbitals of the two sets of H_2,H_3 and H_5,H_6 pairs mimic two bent p orbitals located on the first and second carbons of the methyl groups. This pseudo-out-of-plane π character delocalizes the SOMO on 8 of the 10 atoms. It is a form of hyperconjugation where unpaired electron and its spin density migrate from the NO group to the two CH_3 groups, as shown in Figure 5. This particular stable configuration of the hydrogen atoms in each methyl group, which favors hyperconjugation, will be referred to as **C1**.

3.2. Stable Conformations of Radicals Containing One and Two CH_3 or CF_3 Groups. The simplest form of hyperconjugation due to a single methyl group occurs in the ethyl radical shown in Figure 6. It arises when the H_1 and H_2 atomic orbitals have the same phase, whereas H_3 has an opposite phase. In this most stable configuration, H_1 and H_2 are above the $C_1C_2H_4H_5$ plane, and H_3 is below the plane. This is referred to as **C2** configuration. In this case, H_4 and H_5 also lie in the plane,

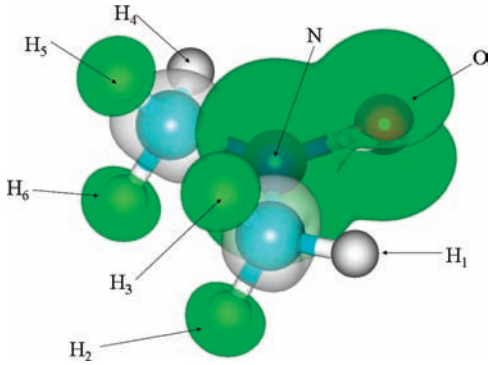

Figure 5. Three-dimensional contours of the **DMNO·** radical's net spin density. Positive spin density contours are in green and the negative spin density clouds are in white.

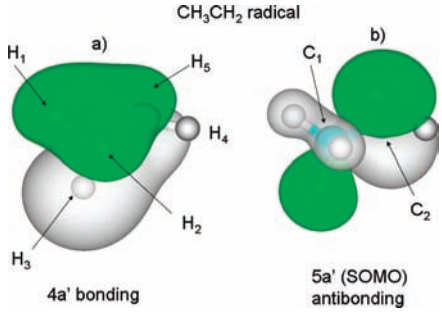

Figure 6. (a) Three-dimensional plot of the one-electron 4a′ valence orbital exhibiting hyperconjugation. (b) Corresponding antibonding combination of 5a′ singly occupied molecular orbital.

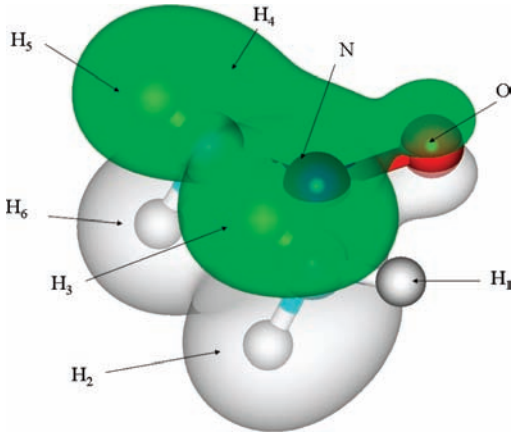

Figure 7. Three-dimensional contours of the DMNO radical's $1b_1$ one-electron orbital. Positive spin density contours are in green, and the negative spin density clouds are in white.

are nonbonding, and are not involved in the delocalization. In the **C2** configuration, the s(H_1), s(H_2), and s(H_3) orbitals combine to form a π-type orbital that can interact with the $2p_z(C_2)$ orbital of the CH_2 group. This out-of-plane combination is bonding in the 4a′ mo (Figure 6a), causes extensive delocalization over the radical, and stabilizes it. The corresponding antibonding combination occurs in the 5a′ SOMO shown in Figure 6b.

The **DMNO·** radical contains two CH_3 groups that have a **C1**-type orientation. The [s(H_2), s(H_3)] pair from the first CH_3 group and [s(H_5), s(H_6)] pair from the second CH_3 group combine to form two π-type orbitals, shown in Figure 7. The appropriate alignment of the four hydrogen atoms is crucial to form the proper combination of atomic orbitals that interact with the NO π orbital and results in delocalization over the entire molecule. Consequently, the preferred conformation is when

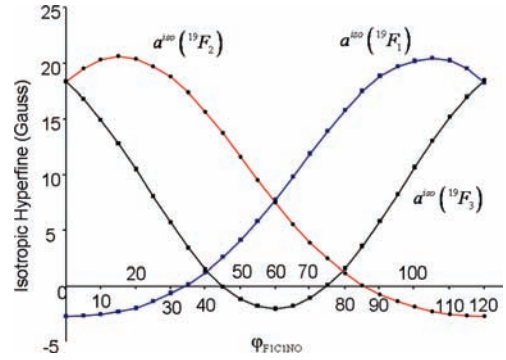

Figure 8. Variation of the **TFMNO·** $a^{iso}(^{19}F_1)$, $a^{iso}(^{19}F_2)$, and $a^{iso}(^{19}F_3)$ as a function of the F_1C_1NO dihedral angle.

H_1 and H_4 lie in the C_1C_2NO plane, as depicted in Figures 4, 5, and 7. In specific, the electron density of H_3, C_1, NO, C_2, and H_5 form a bonding combination above the C_1, C_2, N, O plane, whereas H_2, C_1, NO, C_2, and H_6 form another below the plane. The bonding nature of the $1b_1$ valence one-electron molecular orbital, in Figure 7, is the cause of the stabilization due to hyperconjugation.

3.3. Correlated Rotations in the TFMNO· Radical. The next logical step is to investigate the effects of the rotation of one of the **TFMNO·** radical's CF_3 groups on the other. Because the six F atoms are larger than the H atoms of **DMNO·**, their effects are predicted to be much more significant.

First, the C_1, C_2, N, and O atoms were all forced to lie in one plane. The same relaxed scan procedure used for **DMNO·** was then also followed for the **TFMNO·** radical, shown in Figure 1. The F_1C_1NO dihedral angle ($\varphi_{F_1C_1NO}$) was varied from 0 to 120°. Initially, $\varphi_{F_1C_1NO}$ was set to 0°, and the other internal coordinates were optimized. Once partial optimization was complete, the six $a^{iso}(^{19}F)$ and $a^{iso}(^{14}N)$ were computed using the EPR-II basis set and the UB1LYP functional. The partial optimization and hyperfine tensor components were determined again after F_1C_1NO was increased by 5°. This resulted in the curves given in Figure 8.

A comparison of Figures 3 and 8 shows that the [$a^{iso}(^1H_1)$, $a^{iso}(^1H_2)$, $a^{iso}(^1H_3)$] and [$a^{iso}(^{19}F_1)$, $a^{iso}(^{19}F_2)$, $a^{iso}(^{19}F_3)$] sets display similar behavior as $\varphi_{F_1C_1NO}$ is varied from 0 to 120°. Because it was shown in Section 3.1 that the $a^{iso}(^1H_1)$, $a^{iso}(^1H_2)$, and $a^{iso}(^1H_3)$ of **DMNO·** obey the McConnell relation given by eq 3, then one may also conclude that this is also the case for **TFMNO·.**

This, at first, may seem to be counterintuitive because the **TFMNO·** fluorine frontier orbitals are p in character, whereas those of the **DMNO·** hydrogens are s in nature. However, the plot of the **TFMNO·** SOMO, in Figure 9, reveals that the 2p orbitals of F_2, F_3, F_5, and F_6 are hybridized to form new σ-type p orbitals that are directed toward the carbon atoms of the corresponding C−F bonds. They are identified in Figure 9 by four arrows. The lobes of these hybridized $p_\sigma(F_2)$, $p_\sigma(F_3)$, $p_\sigma(F_5)$, and $p_\sigma(F_6)$ orbitals that face the carbon atoms, when viewed along their corresponding C−F bonds, have cylindrical symmetry and are effectively equivalent to the corresponding s(H_2), s(H_3), s(H_5), and s(H_6) orbitals of **DMNO·** in Figure 5.

Figure 9 shows the carbon and nitrogen orbitals of the SOMO bonding with respect to one another. In addition, the carbon-facing lobes of $p_\sigma(F_2)$ and $p_\sigma(F_3)$ have opposite phases and form a p-type orbital perpendicular to the C_1C_2NO plane. This out-of-plane p-type orbital interacts with the bonding combination of the p(C_1) and p(N) orbitals. The $p_\sigma(F_5)$ and $p_\sigma(F_6)$ lobes form a similar p-type orbital that also interacts with the p(C_2)−p(N)

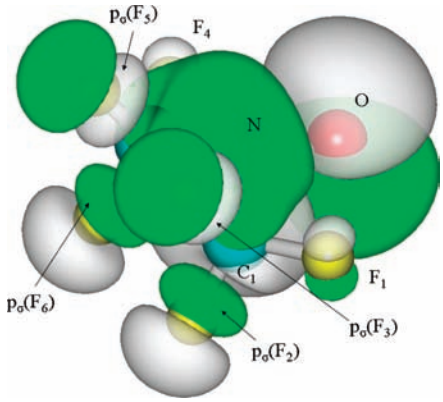

Figure 9. Three-dimensional isosurface of the **TFMNO·** SOMO. Green surfaces have a positive phase, whereas the white surfaces are negative. The molecule has the same orientation as that in Figure 1. The F_1C_1NO dihedral angle is zero. Arrows point to the lobes of the $p_\sigma(F_2)$, $p_\sigma(F_3)$, $p_\sigma(F_5)$, and $p_\sigma(F_6)$ orbitals that face the carbon atoms.

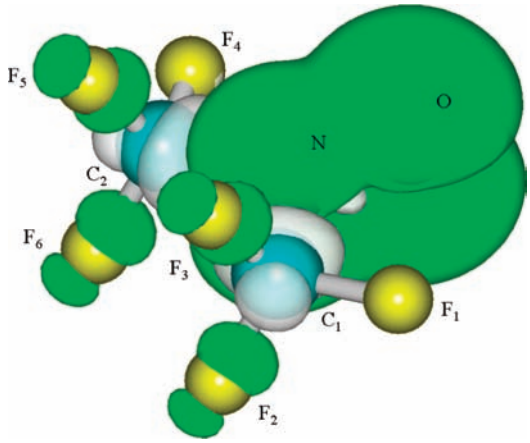

Figure 10. Three-dimensional contours of the net spin density of the **TFMNO·** radical. Negative spin density clouds are in white, whereas positive spin density contours are in green.

orbital combination. This interaction above and below the C_1C_2NO plane is a classical case of hyperconjugation that induces delocalization, as illustrated in the spin density plot of Figure 10. Consequently, aside from the outermost lobes on the fluorine atoms, the net spin density in Figure 10 is very similar to that in Figure 5.

For the sake of completeness, one should note that the F_1 and F_4 atoms, in Figure 9, lie in the C_1C_2NO plane and have pure p character. Their net spin density at the nucleus is only due to core polarization. From this, one concludes that the hyperconjugation in **TFMNO·** exists and is very similar to that of the **DMNO·** radical.

The $a^{iso}(^{19}F_1)$, $a^{iso}(^{19}F_2)$, and $a^{iso}(^{19}F_3)$ as a function of $\varphi_{F_1C_1NO}$ in Figure 8 also display perfect conformity with the McConnell relation of eq 3. This means that as the first CF_3 group is forced to rotate from 0 to 120°, its three F−C−F angles remain the same and do not change or get distorted.

In contrast with $a^{iso}(^{19}F_1)$, $a^{iso}(^{19}F_2)$, and $a^{iso}(^{19}F_3)$, which have a behavior similar to that of $a^{iso}(^{1}H_1)$, $a^{iso}(^{1}H_2)$, and $a^{iso}(^{1}H_3)$ of **DMNO·** as their dihedral angles are varied, $a^{iso}(^{19}F_4)$, $a^{iso}(^{19}F_5)$, and $a^{iso}(^{19}F_6)$ behave very differently from $a^{iso}(^{1}H_4)$, $a^{iso}(^{1}H_5)$, and $a^{iso}(^{1}H_6)$. In this case, the relaxed scan is predominantly influenced by two competing factors. The first is the "geared" CR between both CF_3 groups. The fluorine atoms from different CF_3 groups are close enough such that steric repulsion between them causes them to avoid one another. As the first CF_3 rotates,

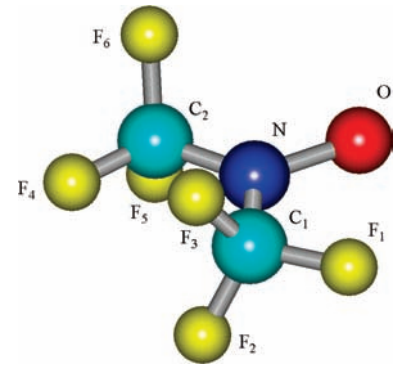

Figure 11. Initial configuration of the TFMNO· trifluoromethyl groups with $\varphi_{F_1C_1NO} = 0°$ and $\varphi_{F_4C_2NO} = 180°$.

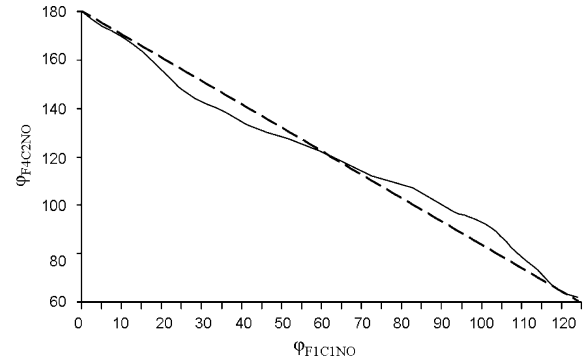

Figure 12. Effect of rotation of the **TFMNO·** radical's first CF_3 group on the three $a^{iso}(^{19}F)$ of the second.

it causes the second CF_3 group to rotate as well. This is very similar to two interlocked gears where one drives the other and vice versa. The second factor is the appropriate orientation (**C1** or **C2** conformations) of the two CF_3 groups with respect to the NO π-electron cloud to maximize hyperconjugation and stabilization. An additional third less-important factor is the delocalization of the electron density between the two CF_3 groups.

The interplay of these effects is best demonstrated when one starts with **TFMNO·** in the configuration shown in Figure 11. The difference between the **TFMNO·** conformations in Figures 10 and 11 is that the second CF_3 group is rotated by 180°. In Figure 11, **TFMNO·** has an energy minimum with the dihedral angles $F_1C_1NO = 0°$ and $F_4C_2NO = 180°$. Here the orientations of the two CF_3 groups are of the **C1** type.

If perfect gearing was the only factor, then a plot of the $\varphi_{F_4C_2NO}$ dihedral angle against $\varphi_{F_1C_1NO}$ would result in the straight dashed line in Figure 12. In the $\varphi_{F_1C_1NO} = 0$ to 15° region, when the first CF_3 group is rotated, it forces the second CF_3 group, via gearing, to follow closely. Therefore, both the dashed and solid lines in Figure 12 are close to one another in this range. However, when the first CF_3 group is forced to rotate beyond 15°, it loses its **C1** alignment with the NO π orbital. This decreases its ability to delocalize via hyperconjugation and tends to destabilize the radical. In addition, the second CF_3 has a tendency to rotate on its own so that the C−F_6 bond becomes perpendicular to the C_1C_2NO plane with $\varphi_{F_4C_2NO} = 150°$. The resulting **C2** orientation increases the overlap between the second CF_3 group and the NO π-orbital, maximizes hyperconjugation, and stabilizes the radical. As a result, the solid line in Figure 12, drops below the dashed one. In the range of $\varphi_{F_1C_1NO} = 30-45°$, the first CF_3 group forces the second one to rotate further but is opposed by the latter's stable **C2** conformation. This causes the two lines to get closer together. Between $\varphi_{F_1C_1NO}$

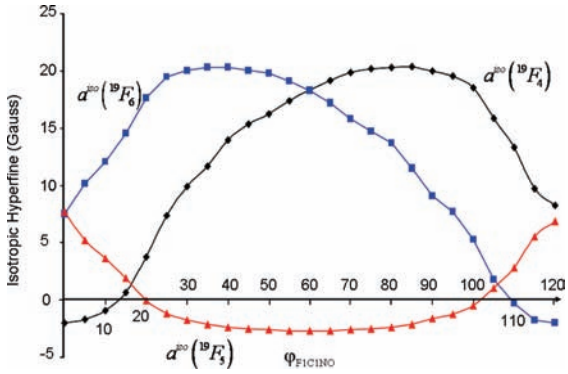

Figure 13. Plot of the $\varphi_{F_4C_2NO}$ dihedral angle obtained from the relaxed geometry optimizations as $\varphi_{F_1C_1NO}$ is varied from 0 to 120°.

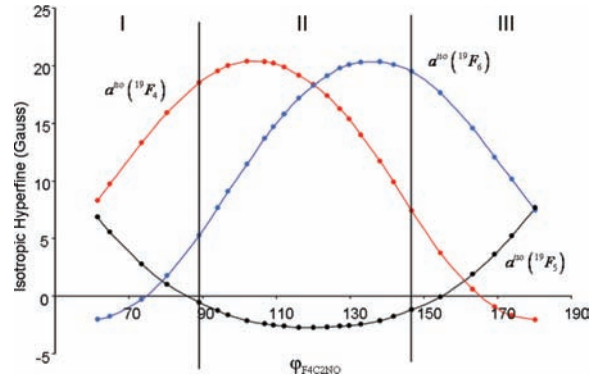

Figure 14. Scatter plot of the **TFMNO**· $a^{iso}(^{19}F_4)$, $a^{iso}(^{19}F_5)$, and $a^{iso}(^{19}F_6)$ as a function of the F_4C_2NO dihedral angle.

= 45 and 60°, both gearing and hyperconjugation reinforce one another, and the two lines coincide at 60°.

At $\varphi_{F_1C_1NO}$ = 60°, both CF_3 groups have a **C1** stable configuration, and the radical has become the mirror image of that in Figure 11.

The reasoning used in the region of 0−60° may also be similarly applied to the two lines in the 60−120° region. The interplay between the gearing forces and the specific orientations that lead to stable **C1** and **C2** configurations causes the right-hand side of the curves to be roughly related to the left-hand side by a center of inversion around $\varphi_{F_1C_1NO}$ = 60°. A careful inspection of the plot in Figure 12 shows that although it appears to be symmetric around 60°, it is not perfect. This is understandable because the geometry optimizations of the relaxed scans have finite tolerances. Each optimization is terminated when all criteria given in Table 1 are met. Because of the finite tolerances of these criteria, some small differences in the optimized bond distances and angles occur depending on how the local minimum is approached on the energy surface. In turn, these lead to the small differences in the shape of the solid line below and above 60°. Finally, from Figure 12, it is also clear that as the first CF_3 group rotates by 120° the second one also spans the same angular range.

The variation of $a^{iso}(^{19}F_4)$, $a^{iso}(^{19}F_5)$, and $a^{iso}(^{19}F_6)$ as $\varphi_{F_1C_1NO}$ is scanned from 0 to 120° is given in Figure 13. The plots also show almost perfect symmetry of $a^{iso}(^{19}F_4)$, $a^{iso}(^{19}F_5)$, and $a^{iso}(^{19}F_6)$ around 60°. The small differences between the ranges of 0−60° and 60−120° are again attributed to the finite tolerances in geometry optimization.

Although at first glance, Figure 13 does not resemble Figure 8, they are closely related. The isotropic hyperfine coupling constants in both Figures obey the McConnell relation. This is evident when a scatter plot versus $\varphi_{F_4C_2NO}$ is drawn in Figure 14 and compared with Figure 8. The shapes of the curves in the two Figures are similar, but the points in Figure 14 are not equidistantly spaced as in Figure 8. They are compressed in the middle region compared with the outer ones demarcated by the vertical lines. This is due to the angular deviations from linearity caused by hyperconjugation, as shown in Figure 12.

Figures 13 and 14 show that the values show that $a^{iso}(^{19}F_4)$, $a^{iso}(^{19}F_5)$, and $a^{iso}(^{19}F_6)$ also permute in a cyclical manner, as dictated by a 120° rotation. Therefore, unlike the **DMNO**· radical, where second CH_3 group undergoes a rocking motion of 7°, the second CF_3 group undergoes full rotation.

In summary, one concludes that gearing plays a predominant role in how the rotation of one CF_3 group affects the other. This gearing is further influenced and modulated by forces due to the stable **C1** and **C2** conformations from both CF_3 groups due to hyperconjugation.

From the present calculations the rotational energy barrier is found to be ~50 cm^{-1}. This is low and may easily be overcome in the temperature range of 163−297 K. One may use bond orders, derived from a population analysis, in a strictly qualitative fashion to describe the type of bond formed between two atomic centers. A Mayer population analysis at each rotation angle indicates that the **TFMNO**· C_1−N and C_2−N bond orders span a range from 0.91 to 0.95 as the two CF_3 groups are rotated from 0 to 120°. Therefore, the C−N bonds are effectively single bonds. This confirms the observations by Scheidler and Bolton that the EPR intensities of the fluorine hyperfine splittings should obey a binomial distribution characteristic of six equivalent fluorine atoms and that the rotation rate must be much larger than that of the X-band (9.0 GHz) EPR experimental time scale.[8]

To compare the numerical values of the rotationally averaged hyperfine coupling constants with experiment at ambient temperatures, the Maxwell−Boltzman distribution is applied. The total energy of the optimized geometries, $E_{TOT}(\varphi_{F_1C_1NO})$, is used to find the probability, $p(\varphi_{F_1C_1NO})$, that the radical exists in a certain conformation with a specific angle, $\varphi_{F_1C_1NO}$. This is obtained from[12,22]

$$p(\varphi_{F_1C_1NO}) = \frac{\exp\left(-\frac{E_{TOT}(\varphi_{F_1C_1NO})}{kT}\right)}{\sum_{\varphi_{F_1C_1NO}=0}^{120} \exp\left(-\frac{E_{TOT}(\varphi_{F_1C_1NO})}{kT}\right)} \quad (4)$$

which is subsequently used to find the averaged isotropic hyperfine coupling constants via the mean value expression

$$\langle a^{iso} \rangle = \frac{\sum_{\varphi_{F_1C_1NO}=0}^{120} p(\varphi_{F_1C_1NO}) a^{iso}(\varphi_{F_1C_1NO})}{\sum_{\varphi_{F_1C_1NO}=0}^{120} p(\varphi_{F_1C_1NO})} \quad (5)$$

Table 2 lists the rotationally averaged ^{14}N HFCC, $\langle a^{iso}(^{14}N)\rangle$, determined from eqs 4 and 5 as a result of the rotation ranging from 0 to 120° at T = 298.18 K. When all C_1, C_2, N, and O atoms lie in the same plane (bend angle = 0), the $\langle a^{iso}(^{14}N)\rangle$ is 6.010 G. It is lower than the experimental value of 9.3 G.[7] This is understandable because in the planar case, $\langle a^{iso}(^{14}N)\rangle$ arises only from core polarization. In its most stable geometry, the C_1, C_2, N, and O atoms are not planar. In an actual experiment,

TABLE 2: Averaged Hyperfine Coupling Constants (*G*) of the TFMNO· Radical at $T = 298.18$ K

	exptl (*G*)	calcd (*G*)	
bend angle		0.0	15.0
$\langle a^{iso}(^{14}N)\rangle$	9.30	6.010	7.785
$\langle a^{iso}(^{19}F_{1-3})\rangle$		7.993	7.375
$\langle a^{iso}(^{19}F_{4-6})\rangle$		8.351	7.490
$\langle a^{iso}(^{19}F_{1-6})\rangle$	8.20	8.172	7.432

the oxygen atom of the NO moiety will also vibrate out of the C_1-C_2-N plane. This will induce additional s(N) character, leading to an increase in the net spin density on the ^{14}N nucleus and a larger $\langle a^{iso}(^{14}N)\rangle$. The entire set of calculations for **TFMNO·** was repeated as a function of the out-of-plane NO bend angle. Indeed, at $T = 298.18$ K, $\langle a^{iso}(^{14}N)\rangle$ increases as the bend angle increases. The total energy minimum occurs when the bend angle is ~15°. The corresponding $\langle a^{iso}(^{14}N)\rangle$ is 7.785 G and increases to 8.549 at 20°. At an angle of 25°, which is only 10° away from the equilibrium geometry, $\langle a^{iso}(^{14}N)\rangle = 9.865$ G, which is larger than the experimental value by ~0.565G. The main aim of the article is not to reproduce the experimental results as accurately as possible but to understand the rotational aspects of the molecule and how they are affected by gearing and hyperconjugation.

The rotationally averaged values of the two CF_3 groups are also listed in Table 2. Because in this study the first CF_3 group is forced to rotate by equal increments of 5° and the second CF_3 group responds to this rotation, they are not expected to give the same $\langle a^{iso}(^{19}F)\rangle$. At the equilibrium geometry, the rotationally averaged HFCC for the first group, $\langle a^{iso}(^{19}F_{1-3})\rangle$, is 7.375 G, whereas that of the second, $\langle a^{iso}(^{19}F_{4-6})\rangle$, is 7.490 G. The rotationally averaged value of both CF_3 groups is 7.432 G. This is within 1.0 G of the experimentally estimated value of 8.200 G.

From these extensive sets of calculations, the rotational energy barrier is estimated to be 48.76 cm^{-1}, and the out-of-plane NO bending mode is ~216.83 cm^{-1}. The probability of finding **TFMNO·** in its *j*th vibrational state is given by

$$p_j = \frac{\exp\left\{-\frac{hc\bar{\nu}_j}{kT}\right\}}{q^V} \tag{6}$$

where $\bar{\nu}_j$ is the vibrational wavenumber and q^V is the corresponding vibrational partition function. Assuming a simple harmonic oscillator model and temperatures above 50 K, this last expression may be approximated as

$$p_j = \exp\left\{-\frac{jhc\bar{\nu}}{kT}\right\}\left[1 - \exp\left\{-\frac{hc\bar{\nu}}{kT}\right\}\right] \tag{7}$$

From eq 7, it is found that as the temperature is increased from 163 to 297 K, the probability of finding the radical in its lowest out-of-plane vibrational state drops from 84 to 63%. In contrast, the probability that it exists in its first out-of-plane vibrational excited state increases from 13.7 to 23%. The probability density, $|\psi_V(d_{NO})|^2$, for the first excited state is a maximum when its out-of-plane NO bending mode amplitude, d_{NO}, is larger than that of the ground state. Therefore, as the temperature rises, one expects the out-of-plane NO bending mode amplitude to increase, leading to a larger $\langle a^{iso}(^{14}N)\rangle$ and a smaller $\langle a^{iso}(^{19}F_{1-6})\rangle$. This is the same trend experimentally found by Scheidler and Bolton[8] and expressed in eqs 1 and 2.

As expected, the rotational and vibrational modes are coupled, and we have not taken into account the coupling between these modes. Further improvement of the computed HFCCs may be accomplished by double averaging over rotations coupled to out-of-plane NO displacement vibrations. These types of computational averaging procedures are not trivial and computationally expensive. They are presently being developed in our laboratory. In addition, more recent and specialized basis sets, such as Barone's N07D,[23,24] and the parameter-free PBE0 hybrid density functionals[17] may also narrow the numerical differences. The inclusion of solvent effects derived from the PCM[24,25] and COSMO[26] models should also improve the agreement between computed and experimental values.

4. Summary and Conclusions

The correlated averaging of the CH_3 and CF_3 groups on the electronic structure and nuclear hyperfine coupling constants of **DMNO·** and **TFMNO·** have been investigated. In the **TFMNO·** case, the influence of out-of-plane NO vibrations on $a^{iso}(^{14}N)$ and $\langle a^{iso}(^{19}F)\rangle$ are also studied.

When the first CH_3 group in **DMNO·** is forced to rotate, its $a^{iso}(^1H_1)$, $a^{iso}(^1H_2)$, and $a^{iso}(^1H_3)$ are found to obey the McConnell relation.[20] Their calculated B_0 and B_1 constants in eq 3 are approximately −1.1 and 44.0 G, respectively. The effect of rotation of one CH_3 group on the other is of minor importance. The two methyl groups do not gear with each other, but changing $\varphi_{H_1C_1NO}$ of the first CH_3 group induces only a small rocking effect of ~7° in the second CH_3 group. Hyperconjugation in **DMNO·** plays a significant role in the delocalization of the SOMO from the NO moiety to the two methyl groups.

The variation of $a^{iso}(^{19}F_1)$, $a^{iso}(^{19}F_2)$, and $a^{iso}(^{19}F_3)$ as a function of $\varphi_{F_1C_1NO}$ in**TFMNO·** also obeys the McConnell relation of eq 3. Therefore, as the first CF_3 group is forced to rotate from 0 to 120°, its three F−C−F angles remain the same and do not significantly change or distort.

Unlike the **DMNO·** radical, where the second CH_3 group undergoes a slight rocking motion, the second CF_3 group undergoes full rotation. Therefore, $a^{iso}(^{19}F_4)$, $a^{iso}(^{19}F_5)$, and $a^{iso}(^{19}F_6)$ do not behave like $a^{iso}(^1H_4)$, $a^{iso}(^1H_5)$, and $a^{iso}(^1H_6)$. The fluorine atoms from different CF_3 groups are close enough to avoid one another. The steric repulsion between the CF_3 groups causes them to act as two interlocked gears where one drives the other and vice versa. One concludes that gearing plays a predominant role in how the rotation of one CF_3 group affects the other.

The second major factor that affects the magnitudes of the nuclear hyperfine coupling constants during averaging is stabilization due to hyperconjugation. At the appropriate **C1** or **C2** orientations, the CF_3 groups a have large overlap with the NO π-electron cloud leading to stable configurations. Hyperconjugation in **TFMNO·** occurs because the lobes of the hybridized $p_\sigma(F_2)$, $p_\sigma(F_3)$, $p_\sigma(F_5)$, and $p_\sigma(F_6)$ orbitals that face the carbon atoms, when viewed along their corresponding C−F bonds, have cylindrical symmetry and are of the correct phases, as shown in Figure 9. A comparison of Figures 5 and 9 indicates that the $p_\sigma(F_2)$, $p_\sigma(F_3)$, $p_\sigma(F_5)$, and $p_\sigma(F_6)$ orbitals are effectively equivalent to the corresponding $s(H_2)$, $s(H_3)$, $s(H_5)$, and $s(H_6)$.

The **TFMNO·** C_1-N and C_2-N bond orders range from 0.91 to 0.95 as the two CF_3 groups are rotated. Therefore, the C−N bonds are essentially single bonds. This, in conjunction with the low rotational energy barrier (~50 cm^{-1}), confirms the observations by Scheidler and Bolton that the X-band EPR

intensities of the fluorine hyperfine splittings, in the range of 163−297 K, should obey a binomial distribution characteristic of six equivalent fluorine atoms.

The calculations show that as the temperature increases, the out-of-plane NO bending mode amplitudes increase and lead to larger $<a^{iso}(^{14}N)>$ values. It also results in smaller $<a^{iso}(^{19}F_{1-6})>$ values. This follows and corroborates the experimental findings of Scheidler and Bolton.[8]

Acknowledgment. This article is dedicated to Dr. James R. Bolton for his long and outstanding contribution to the field of electron paramagnetic resonance. S.M. is grateful to the Natural Sciences and Engineering Research Council of Canada for financial support in the form of Discovery (Operating) grants. J.S. thanks the University of New Brunswick for Graduate Student funding. We are also grateful to Professor Frank Neese for the use of his ORCA suite of programs.

References and Notes

(1) Murib, J. H.; Ritter, D. M. *J. Am. Chem. Soc.* **1952**, *74*, 3394–3398.
(2) Berliner, L. J. *Biological Magnetic Resonance: Spin Labeling in the Next Millenium*; Plenum Press: New York, 1998.
(3) Edwards, T. E.; Okonogi, T. M.; Robinson, B. H.; Sigurdsson, S. T. *J. Am. Chem. Soc.* **2001**, *123*, 1527–1528.
(4) Griffith, O. H.; Waggoner, A. S. *Acc. Chem. Res.* **1969**, *2*, 17–24.
(5) Kocherginsky, N.; Swartz, H. M. *Nitroxide Spin Labels, Reactions in Biology and Chemistry*; CRC Press: Boca Raton, FL, 1995.
(6) Zhang, Z.; Berg, A.; Levanon, H.; Fessenden, R. W.; Meisel, D. *J. Am. Chem. Soc.* **2003**, *125*, 7959–7963.
(7) Blackley, W. D.; Reinhard, R. R. *J. Am. Chem. Soc.* **1965**, *87*, 802–805.
(8) Scheidler, P. J.; Bolton, J. R. *J. Am. Chem. Soc.* **1966**, *88*, 371–373.
(9) Improta, R.; Barone, V. *Chem. Rev. (Washington, DC, U.S.)* **2004**, *104*, 1231–1253.
(10) Pavone, M.; Cimino, P.; DeAngelis, F.; Barone, V. *J. Am. Chem. Soc.* **2006**, *128*, 4338–4347.
(11) Mattar, S. M. *Chem. Phys. Lett.* **2006**, *427*, 438–442.
(12) Mattar, S. M.; Sanford, J. *J. Phys. Chem. A* **2008**, *112*, 11349–11354.
(13) Mattar, S. M.; Stephens, A. D. *J. Phys. Chem. A* **2000**, *104*, 3718–3732.
(14) Mattar, S. M.; Stephens, A. D. *Chem. Phys. Lett.* **2000**, *319*, 601–610.
(15) Neese, F. *ORCA*, an abinitio, density functional and semiempirical program package; University of Bonn: Bonn, Germany, 2007.
(16) Adamo, C.; Barone, V. *Chem. Phys. Lett.* **1997**, *274*, 242–250.
(17) Adamo, C.; Barone, V. *J. Chem. Phys.* **1999**, *110*, 6158–6170.
(18) Perdew, J. P.; Burke, K.; Ernzerhof, M. *Phys. Rev. Lett.* **1997**, *78*, 1396.
(19) Barone, V. *Recent Advances in Density Functional Methods 361*; World Scientific: Singapore, 1995.
(20) Heller, C.; McConnell, H. M. *J. Chem. Phys.* **1960**, *32*, 1535–1539.
(21) Mattar, S. M.; Emwas, A. H.; Stephens, A. D. *Chem. Phys. Lett.* **2002**, *363*, 152–160.
(22) Mattar, S. M.; Sanford, J. *Chem. Phys. Lett.* **2006**, *425*, 148–153.
(23) Barone, V.; Cimino, P. *Chem. Phys. Lett.* **2008**, *454*, 139–143.
(24) Cossi, M.; Scalmani, G.; Rega, N.; Barone, V. *J. Chem. Phys.* **2002**, *117*, 43–54.
(25) Williams, F.; Chen, G. F.; Mattar, S. M.; Scudder, P. H.; Trieber, D. A.; Saven, J. G.; Whritenour, D. C.; Cimino, P.; Barone, V. *J. Phys. Chem. B* **2009**, *113*, 9026–9034.
(26) Sinnecker, S.; Rajendran, A.; Klamt, A.; Diedenhofen, M.; Neese, F. *J. Phys. Chem. A* **2006**, *110*, 2235–2245.

JP9076646